SICE Annual Conference 2012
August 20-23, 2012, Akita University, Akita, Japan

Analyses of Jumping Motion of Humanoid Robot Using Arms' Swinging

Jumpei Nishiguchi[1], Mamoru Minami[1], Akira Yanou[1], Takayuki Matsuno[1] and Tomohide Maeba[1]

[1]Graduate School of Natural Science and Technology, Okayama University, Okayama, Japan
(Tel: +81-86-251-8924; E-mail: yanou@qumi.sys.okayama-u.ac.jp)

Abstract: The objective of this research is to analyze humanoid's jumping and landing motions on a view point of arms' dynamical coupling onto jumping. Humans seem to use arms' swinging for walking or running effectively and jump highly by swinging up arms high. So, we gave input torques to arms in such a way as to swing arms similar to humans, and changed timing to start swinging them, comparing them with humanoid's motion that does not swing the arms through numerical simulation. Then we have confirmed that appropriate swinging motions of arms help the jumping to be higher than those without arms' swinging.

Keywords: Vertical jump, Constraint motion, Arms' swing.

1. INTRODUCTION

Human uses arms effectively in various situations, which indicates that we can control humanoid robot effectively by using dynamical coupling of arms. However, there is little study about arms' beneficial use. Therefore, we focus on humanoid's motion with arms' swing.

Although model of humanoid is simplified in lots of studies, [1] considers many kinds of gaits including point-contacting and surface-contacting of feet. Our research has begun from such view point of [1] as aiming at describing gait's dynamics as correctly as possible.

There are two different approaches of humanoid researches such as a real experiment view point and simulation-based one when discussing dynamical walking motion of robot. Using software simulation, it may fall in meaningless discussions unless the dynamical model describes correctly the real physical dynamical behavior. In line with this thinking way, we have discussed a dynamical model of humanoid's walking motion including slipping, bumping and tipping [2]. Using correct model, simulations enables us to obtain every piece of data without real sensors and can discuss about phenomenon being hard to obtain from real machine, e.g. falling and crashing to floor when walking and jumping. So we think simulation is a convenient tool in discussing complicated walking dynamics before realizing real robot's walking.

We made humanoid's model which can describe jumping and landing motions while utilizing dynamical couplings of arms' swinging. Although in [3] and [4] human jumping has been modeled, both models never contain arms and then arms' influence is out of concerns. In vertical jump, human swings up of arms from lower position and makes them stop at head's height to jump highly. So we gave input to arms in such a way as to perform above mentioned arms' swing motion, and simulated jumping motion of humanoid robot. The results show that the humanoid robot can jump higher than without them. Moreover, this report explored jumping motion simulations with various timing to starting swinging the arms, and discusses conditions that the humanoid can jump highly by verifying the motions through contacting normal force against ground and motion energy.

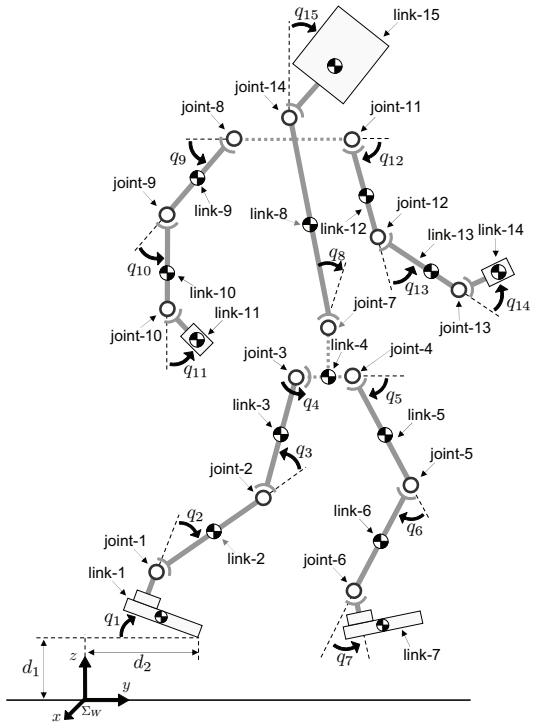

Fig. 1 Model of humanoid robot

2. DYNAMICAL HUMANOID MODEL OF JUMPING

Humanoid model and definition of joint angle q_i and position d_i are shown in Fig. 1. Our model represents rigid whole body—feet, torso, arms and so on—having 17 degree-of-freedom.

In this paper, link-1 is defined as "supporting-foot" and link-7 is defined as "floating-foot" or "contacting-foot" according to the walking state.

PR0001/12/0000- 0496¥400

2.1 Derivation of equation of motion by Newton-Euler method

We derive the dynamics of humanoid being simulated as a serial link manipulator having ramifications by Newton-Euler method [7]. We derive equation of motion based on each coordinate system Furthermore equation of motion about position d_1 and d_2 are derived as two prismatic links which length is d_1 and d_2.

We first have to calculate relations of positions, velocities and accelerations between links as forward kinematics procedures from bottom link to top link. Serial link's acceleration of the origin ${}^i\ddot{\boldsymbol{p}}_i$ and acceleration of the center of mass ${}^i\ddot{\boldsymbol{s}}_i$ based on Σ_i fixed at link-i are obtained as follows.

$$ {}^i\ddot{\boldsymbol{p}}_i = {}^{i-1}\boldsymbol{R}_i^T \left\{ {}^{i-1}\ddot{\boldsymbol{p}}_{i-1} + {}^{i-1}\dot{\boldsymbol{\omega}}_{i-1} \times {}^{i-1}\hat{\boldsymbol{p}}_i + {}^{i-1}\boldsymbol{\omega}_{i-1} \times ({}^{i-1}\boldsymbol{\omega}_{i-1} \times {}^{i-1}\hat{\boldsymbol{p}}_i) \right\} \quad (1) $$

$$ {}^i\ddot{\boldsymbol{s}}_i = {}^i\ddot{\boldsymbol{p}}_i + {}^i\dot{\boldsymbol{\omega}}_i \times {}^i\hat{\boldsymbol{s}}_i + {}^i\boldsymbol{\omega}_i \times ({}^i\boldsymbol{\omega}_i \times {}^i\hat{\boldsymbol{s}}_i) \quad (2) $$

Here, ${}^i\boldsymbol{\omega}_i$ is serial link's angular velocity, ${}^i\dot{\boldsymbol{\omega}}_i$ is angular acceleration, ${}^{i-1}\boldsymbol{R}_i$ means orientation matrix, ${}^{i-1}\hat{\boldsymbol{p}}_i$ represents position vector from the origin of link-$i-1$ to the one of link-i and ${}^i\hat{\boldsymbol{s}}_i$ is defined as gravity center position of link-i.

After the above forward kinematic calculation has been done, contrarily inverse dynamical calculation procedures is the next from top to base link. Newton equation and Euler equation of link-i are represented by Eqs. (3), (4) when ${}^i\boldsymbol{I}_i$ is defined as inertia tensor of link-i.

$$ {}^i\boldsymbol{f}_i = {}^i\boldsymbol{R}_{i+1}{}^{i+1}\boldsymbol{f}_{i+1} + m_i{}^i\ddot{\boldsymbol{s}}_i \quad (3) $$

$$ {}^i\boldsymbol{n}_i = {}^i\boldsymbol{R}_{i+1}{}^{i+1}\boldsymbol{f}_{i+1} + {}^i\boldsymbol{I}_i{}^i\dot{\boldsymbol{\omega}}_i + {}^i\boldsymbol{\omega}_i \times ({}^i\boldsymbol{I}_i{}^i\boldsymbol{\omega}_i) + {}^i\hat{\boldsymbol{s}}_i \times (m_i{}^i\ddot{\boldsymbol{s}}_i) + {}^i\hat{\boldsymbol{p}}_{i+1} \times ({}^i\boldsymbol{R}_{i+1}{}^{i+1}\boldsymbol{f}_{i+1}) \quad (4) $$

Then, rotational equation of motion of link-i is obtained as Eq. (5) by making inner product of induced torque onto the link-i unit vector $\boldsymbol{e}_{z_i} = [0,0,1]^T$ around rotational axis.

$$ \tau_i = (\boldsymbol{e}_{z_i})^T {}^i\boldsymbol{n}_i + D_i\dot{q}_i \quad (5) $$

Finally, we get equation of motion as Eq. (6).

$$ \boldsymbol{M}(\boldsymbol{q})\ddot{\boldsymbol{q}} + \boldsymbol{h}(\boldsymbol{q},\dot{\boldsymbol{q}}) + \boldsymbol{g}(\boldsymbol{q}) + \boldsymbol{D}\dot{\boldsymbol{q}} = \boldsymbol{\tau} \quad (6) $$

$\boldsymbol{M}(\boldsymbol{q})$ is inertia matrix, $\boldsymbol{h}(\boldsymbol{q},\dot{\boldsymbol{q}})$ and $\boldsymbol{g}(\boldsymbol{q})$ are vectors which indicate Coriolis force, centrifugal force and gravity, $\boldsymbol{D} = diag[D_1, D_2, \cdots, D_n]$ is matrix which means coefficients of joints' viscous friction and $\boldsymbol{\tau}$ is input torque. $\boldsymbol{q} = [d_1, d_2, q_1, q_2, \cdots, q_{15}]^T$ is vector which indicate joint angle and position.

2.2 Model of No-foot Contacting the Ground or Single-foot Standing

When we assume humanoid as separate manipulator, we can get equation of motion by discussion of subsection 2.1 as for serial connecting link. However, humanoid of Fig. 1 has two ramifications, so following equations are used as for link-4, 8, 12, 15.

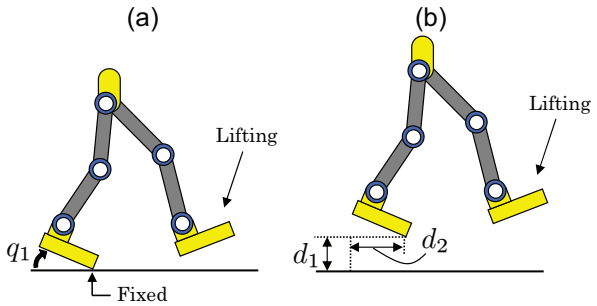

Fig. 2 Phase (IV) and (V)

First, in forward kinematics calculation, velocity and acceleration of link-4 transmit to link-8, so ${}^8\ddot{\boldsymbol{p}}_8$ is obtained as Eq. (7).

$$ {}^8\ddot{\boldsymbol{p}}_8 = {}^4\boldsymbol{R}_8^T \left\{ {}^4\ddot{\boldsymbol{p}}_4 + {}^4\dot{\boldsymbol{\omega}}_4 \times {}^4\hat{\boldsymbol{p}}_8 + {}^4\boldsymbol{\omega}_4 \times ({}^4\boldsymbol{\omega}_4 \times {}^4\hat{\boldsymbol{p}}_8) \right\} \quad (7) $$

On the other hand, velocity and acceleration of link-8 transmit to link-9, link-12 and so ${}^9\ddot{\boldsymbol{p}}_9$ and ${}^{12}\ddot{\boldsymbol{p}}_{12}$ are obtained in a similar way to Eq. (7).

Next, in inverse dynamical calculation, force and torque of both link-5 and link-8 are exerted on link-4, so both effects influence onto link-4 as Eqs. (8), (9).

$$ {}^4\boldsymbol{f}_4 = {}^4\boldsymbol{R}_5{}^5\boldsymbol{f}_5 + {}^4\boldsymbol{R}_8{}^8\boldsymbol{f}_8 + m_4{}^4\ddot{\boldsymbol{s}}_4 \quad (8) $$

$$ {}^4\boldsymbol{n}_4 = {}^4\boldsymbol{R}_5{}^5\boldsymbol{n}_5 + {}^4\boldsymbol{R}_8{}^8\boldsymbol{n}_8 + {}^4\boldsymbol{I}_4{}^4\dot{\boldsymbol{\omega}}_4 + {}^4\boldsymbol{\omega}_4 \times ({}^4\boldsymbol{I}_4{}^4\boldsymbol{\omega}_4) + {}^4\hat{\boldsymbol{s}}_4 \times (m_4{}^4\ddot{\boldsymbol{s}}_4) + {}^4\hat{\boldsymbol{p}}_5 \times ({}^4\boldsymbol{R}_5{}^5\boldsymbol{f}_5) + {}^4\hat{\boldsymbol{p}}_8 \times ({}^4\boldsymbol{R}_8{}^8\boldsymbol{f}_8) \quad (9) $$

Force and torque of both link-9, 12 and 15 are exerted on link-8, so equation of Newton and Euler for link-8 are obtained in a similar way to Eqs. (8), (9).

In terms of equation of motion for humanoid robot, equation of motion Eq. (6) mean the motion standing on single foot like Fig. 2 (a). Here, if supporting-foot is point-contacting and assumed to be without slipping, joint angle can be thought as $\boldsymbol{q} = [q_1, q_2, \cdots, q_{15}]^T \in \boldsymbol{R}^{15}$. This walking pattern is depicted in Fig.2 (a). When supporting-foot should get off the ground as shown in Fig. 2 (b), the state variable for the foot's position d_1 and d_2 are added to $\boldsymbol{q}$, thus $\boldsymbol{q} = [d_1, d_2, q_1, q_2, \cdots, q_{15}]^T \in \boldsymbol{R}^{17}$.

As above stated, in the model of this paper, dimension of variable changes depending on the gate. So, in the following section, when supporting-foot is surface-contacting as shown in Fig. 3 (a), link-1 is considered part of the ground and q_1 can be deleted from $\boldsymbol{q}$, thus $\boldsymbol{q} = [q_2, \cdots, q_{15}]^T \in \boldsymbol{R}^{14}$.

2.3 Model with Point-contacting Constraints

Given a lifting foot contacts with a ground while keeping Phase (IV), Phase (III) appears like Fig. 3 b with the forefoot's z, y-axis position being constrained by the ground. This constraint is represented by Eq. (10), where $\boldsymbol{r}(\boldsymbol{q})$ represents forefoot's position in $\boldsymbol{\Sigma}_W$.

$$ C_{1z}(\boldsymbol{r}(\boldsymbol{q})) = 0, \quad C_{1y}(\boldsymbol{r}(\boldsymbol{q})) = 0 \quad (10) $$

While constrained motion, equation of motion is ob-

tained as Eq. (11)

$$\boldsymbol{M}(\boldsymbol{q})\ddot{\boldsymbol{q}} + \boldsymbol{h}(\boldsymbol{q},\dot{\boldsymbol{q}}) + \boldsymbol{g}(\boldsymbol{q}) + \boldsymbol{D}\dot{\boldsymbol{q}} = \boldsymbol{\tau} + \boldsymbol{j}_{cz}^T f_{nz} + \boldsymbol{j}_{cy}^T f_{cy} \quad (11)$$

f_{nz}, f_{ny} is constraint force, and $\boldsymbol{j}_{cz}^T$, $\boldsymbol{j}_{cy}^T$ are defined as follows.

$$\boldsymbol{j}_{cz}^T = \frac{\left(\frac{\partial C_{1z}}{\partial \boldsymbol{q}^T}\right)^T}{\left\|\frac{\partial C_{1z}}{\partial \boldsymbol{q}^T}\right\|}, \quad \boldsymbol{j}_{cy}^T = \frac{\left(\frac{\partial C_{1y}}{\partial \boldsymbol{q}^T}\right)^T}{\left\|\frac{\partial C_{1y}}{\partial \boldsymbol{q}^T}\right\|} \quad (12)$$

Moreover, Eq. (10) are differentiated by time to times, then we can derive the constraint condition of $\ddot{\boldsymbol{q}}$.

$$\left(\frac{\partial C_{1z}}{\partial \boldsymbol{q}^T}\right)\ddot{\boldsymbol{q}} + \dot{\boldsymbol{q}}^T\left\{\frac{\partial}{\partial \boldsymbol{q}}\left(\frac{\partial C_{1z}}{\partial \boldsymbol{q}^T}\right)\right\}\dot{\boldsymbol{q}} = 0 \quad (13)$$

$$\left(\frac{\partial C_{1y}}{\partial \boldsymbol{q}^T}\right)\ddot{\boldsymbol{q}} + \dot{\boldsymbol{q}}^T\left\{\frac{\partial}{\partial \boldsymbol{q}}\left(\frac{\partial C_{1y}}{\partial \boldsymbol{q}^T}\right)\right\}\dot{\boldsymbol{q}} = 0 \quad (14)$$

The $\ddot{\boldsymbol{q}}$ in Eq. (11), Eq. (13) and Eq. (14) should be identical so the time solution of Eq. (13) and Eq. (14) be under the constraint of Eq. (10). Then the following simultaneous equation of $\ddot{\boldsymbol{q}}$ and the f_{nz}, f_{ny} have to be maintained during the contacting period of the motion. Here, the f_{nz} and f_{ny} are decided dependently to make the $\ddot{\boldsymbol{q}}$ in Eq. (11), Eq. (13) and Eq. (14) to be identical.

$$\begin{bmatrix} \boldsymbol{M}(\boldsymbol{q}) & -\boldsymbol{j}_{cz}^T & -\boldsymbol{j}_{cy}^T \\ \frac{\partial C_{1z}}{\partial \boldsymbol{q}^T} & 0 & 0 \\ \frac{\partial C_{1y}}{\partial \boldsymbol{q}^T} & 0 & 0 \end{bmatrix}\begin{bmatrix} \ddot{\boldsymbol{q}} \\ f_{nz} \\ f_{ny} \end{bmatrix} = \begin{bmatrix} \boldsymbol{\tau} - \boldsymbol{h}(\boldsymbol{q},\dot{\boldsymbol{q}}) - \boldsymbol{g}(\boldsymbol{q}) - \boldsymbol{D}\dot{\boldsymbol{q}} \\ -\dot{\boldsymbol{q}}^T\left\{\frac{\partial}{\partial \boldsymbol{q}}\left(\frac{\partial C_{1z}}{\partial \boldsymbol{q}^T}\right)\right\}\dot{\boldsymbol{q}} \\ -\dot{\boldsymbol{q}}^T\left\{\frac{\partial}{\partial \boldsymbol{q}}\left(\frac{\partial C_{1y}}{\partial \boldsymbol{q}^T}\right)\right\}\dot{\boldsymbol{q}} \end{bmatrix} \quad (15)$$

2.4 Model with Surface-contacting Constraints

When the forefoot's sole surface contacts to the ground as shown Fig. 4 (a), another constraint emerges besides the z-axis constraint C_{1z} and the y-axis constraint C_{1y} defined by Eq. (10) so forefoot's angle has to be kept as zero, that is $C_2(\boldsymbol{r}(\boldsymbol{q})) = 0$, then the plural constraints are

$$\boldsymbol{C}(\boldsymbol{r}(\boldsymbol{q})) = \begin{bmatrix} C_{1z}(\boldsymbol{r}(\boldsymbol{q})) \\ C_{1y}(\boldsymbol{r}(\boldsymbol{q})) \\ C_2(\boldsymbol{r}(\boldsymbol{q})) \end{bmatrix} = \boldsymbol{0}, \quad (16)$$

where in this case $C_2(\boldsymbol{r}(\boldsymbol{q})) = q_e = q_1 + q_2 + \cdots + q_7 = 0$. Then, robot's equation of motion with external forces f_{nz}, f_{ny} and τ_n corresponding to C_{1z}, C_{1y} and C_2 can be derived by the same procedures as Eq. (11):

$$\boldsymbol{M}(\boldsymbol{q})\ddot{\boldsymbol{q}} + \boldsymbol{h}(\boldsymbol{q},\dot{\boldsymbol{q}}) + \boldsymbol{g}(\boldsymbol{q}) + \boldsymbol{D}\dot{\boldsymbol{q}} = \boldsymbol{\tau} + \boldsymbol{j}_{cz}^T f_{nz} + \boldsymbol{j}_{cy}^T f_{ny} + \boldsymbol{j}_r^T \tau_n, \quad (17)$$

where $\boldsymbol{j}_r$ is

$$\boldsymbol{j}_r^T = \left(\frac{\partial C_2}{\partial \boldsymbol{q}^T}\right)^T\left(1/\left\|\frac{\partial C_2}{\partial \boldsymbol{q}^T}\right\|\right). \quad (18)$$

Differentiating by time two times Eq. (16), and combining it with Eq. (17), we get,

$$\begin{bmatrix} \boldsymbol{M}(\boldsymbol{q}) & -\boldsymbol{j}_{cz}^T & -\boldsymbol{j}_{cy}^T & -\boldsymbol{j}_r^T \\ \partial C_{1z}/\partial \boldsymbol{q}^T & 0 & 0 & 0 \\ \partial C_{1y}/\partial \boldsymbol{q}^T & 0 & 0 & 0 \\ \partial C_2/\partial \boldsymbol{q}^T & 0 & 0 & 0 \end{bmatrix}\begin{bmatrix} \ddot{\boldsymbol{q}} \\ f_{nz} \\ f_{ny} \\ \tau_n \end{bmatrix} = \begin{bmatrix} \boldsymbol{\tau} - \boldsymbol{h}(\boldsymbol{q},\dot{\boldsymbol{q}}) - \boldsymbol{g}(\boldsymbol{q}) - \boldsymbol{D}\dot{\boldsymbol{q}} \\ -\dot{\boldsymbol{q}}^T\left\{\frac{\partial}{\partial \boldsymbol{q}}\left(\frac{\partial C_{1z}}{\partial \boldsymbol{q}^T}\right)\right\}\dot{\boldsymbol{q}} \\ -\dot{\boldsymbol{q}}^T\left\{\frac{\partial}{\partial \boldsymbol{q}}\left(\frac{\partial C_{1y}}{\partial \boldsymbol{q}^T}\right)\right\}\dot{\boldsymbol{q}} \\ -\dot{\boldsymbol{q}}^T\left\{\frac{\partial}{\partial \boldsymbol{q}}\left(\frac{\partial C_2}{\partial \boldsymbol{q}^T}\right)\right\}\dot{\boldsymbol{q}} \end{bmatrix}. \quad (19)$$

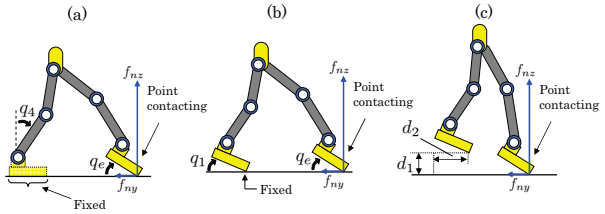

Fig. 3 Phase (II), (III) and (IV')

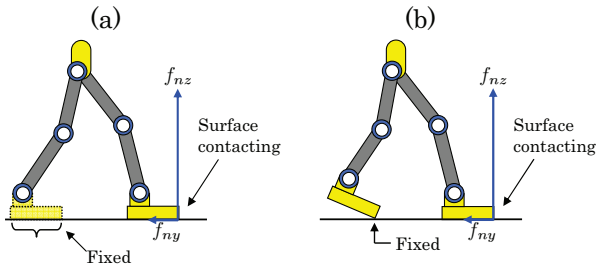

Fig. 4 Phase(I) and (II')

3. JUMPING GAIT TRANSITION

Fig. 5 denotes bipedal jumping gait transition. In the phase that has ramification, the gait is switched to next phase in case of auxiliary written switching condition being satisfied. What the authors want to emphasize here is that the varieties of this transition completely depend on the solution of dynamics shown as Eqs. (6), (15), (19). Therefore, we cannot predetermine the jumping gaits pattern, contrarily it will be depended on the initial conditions of the robot, input torque, the shape of the ground and so on.

3.1 Heel's detaching condition

A condition that heel of supporting-foot detaches from the ground in Fig. 5 (I), (II′) to (II), (III) is discussed. For this judging, ${}^2\boldsymbol{f}_2$ and ${}^2\boldsymbol{n}_2$ calculated from Eqs. 3, 4 in case of $i = 2$ are used. Firstly, coordinates of ${}^2\boldsymbol{f}_2$ and ${}^2\boldsymbol{n}_2$ represented by Fig. 6 (a) are converted from Σ_2 to Σ_W. Then, projection to z-axis of the force and projection to x-axis of the torque are derived by using unit vector $\boldsymbol{e}_x = [1,0,0]^T$ and $\boldsymbol{e}_z = [0,0,1]^T$ as: ${}^W f_{2_z} = \boldsymbol{e}_z^T({}^W\boldsymbol{R}_2\,{}^2\boldsymbol{f}_2)$, ${}^W n_{2_x} = \boldsymbol{e}_x^T({}^W\boldsymbol{R}_2\,{}^2\boldsymbol{n}_2)$ like Fig. 6 (b).

Given that supporting-foot's contacting points are to be two of toe and heel as shown Fig. 6 (c), when forces acting on the toe and heel are defined as f_f, f_r, these forces must satisfy the following equations.

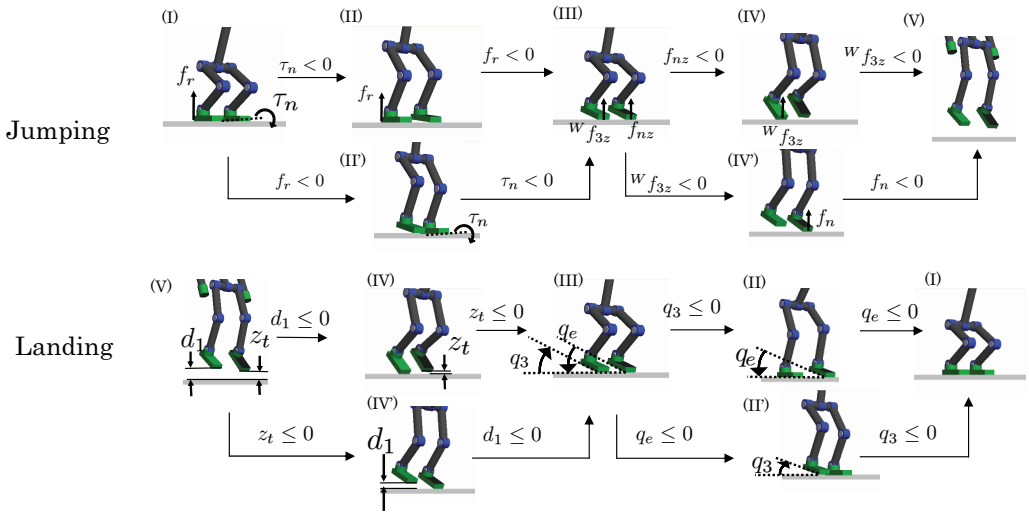

Fig. 5 Phase and gait's transition

$$^W f_{2_z} = f_f + f_r \tag{20}$$

$$^W n_{2_x} = -f_f \cdot l_f + f_r \cdot l_r \tag{21}$$

We can calculate f_f and f_r as Eq. (22) and supporting-foot begins to rotate around the toe like Fig. 6 (d) when value of f_r becomes negative.

$$f_{f,\,r} = \frac{l_r \cdot {}^W f_{2z}}{l_f + l_r} \pm \frac{^W n_{2x}}{l_f + l_r} \tag{22}$$

3.2 Bumping

When floating-foot attaches to ground, we need to consider bumping motion as Fig. 5 (IV) to (III). So we represented completely inelastic collision between foot and the ground by using the method introduced in [1].

First, by integrating Eq. (11) in time, equation of striking moment can be obtained as follows.

$$\boldsymbol{M}(\boldsymbol{q})\dot{\boldsymbol{q}}(t^+) = \boldsymbol{M}(\boldsymbol{q})\dot{\boldsymbol{q}}(t^-) + \boldsymbol{j}_{cz}^T F_{imz} + \boldsymbol{j}_{cy}^T F_{imy} \tag{23}$$

Eq. (23) describes the bumping in z, y-axis of Σ_W between the tiptoe and the ground. $\dot{\boldsymbol{q}}(t^+)$ and $\dot{\boldsymbol{q}}(t^-)$ are angular velocity after and before the strike respectively. $F_{im} = \lim_{t^- \to t^+} \int_{t^-}^{t^+} f_n dt$ means impulse of bumping. Motion of the robot is constrained by the followed equation that is given by differentiating C_1 by time after the strike.

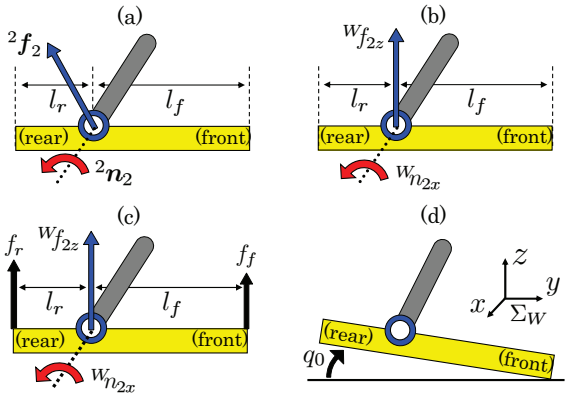

Fig. 6 Force and torque acting on supporting-foot

$$\frac{\partial C_{1z}}{\partial \boldsymbol{q}}\dot{\boldsymbol{q}}(t^+) = 0, \quad \frac{\partial C_{1y}}{\partial \boldsymbol{q}}\dot{\boldsymbol{q}}(t^+) = 0 \tag{24}$$

Then, the equation of matrix formation in the case of heel's bumping can be obtained as follows.

$$\begin{bmatrix} \boldsymbol{M}(\boldsymbol{q}) & -\boldsymbol{j}_{cz}^T & -\boldsymbol{j}_{cy}^T \\ \partial C_{1z}/\partial \boldsymbol{q}^T & 0 & 0 \\ \partial C_{1y}/\partial \boldsymbol{q}^T & 0 & 0 \end{bmatrix} \begin{bmatrix} \dot{\boldsymbol{q}}(t^+) \\ F_{imz} \\ F_{imy} \end{bmatrix} = \begin{bmatrix} \boldsymbol{M}(\boldsymbol{q})\dot{\boldsymbol{q}}(t^-) \\ 0 \\ 0 \end{bmatrix} \tag{25}$$

4. NUMERICAL SIMULATION

This section describes about input torque for jumping and simulation outcome. Under the environment that sampling time was set as 3.0×10^{-3} [sec]. In regard to simulation environment, we used "Borland C++ Builder Professional Ver. 5.0" to compile simulation program and "OpenGL" to display humanoid robot's time-transient configurations.

4.1 Input torque

Three kinds of input torque for jumping, landing and in the air are given.

Input torque for jumping is presented as Eqs. (26) $\sim$ (29). $\boldsymbol{J}_h$ is Jacobian matrix from supporting-foot to head. $\boldsymbol{f}_h$ is force that tries to pull head toward upper direction as Eq. (27), k_{ph} is proportional gain, y_h head position in traveling direction, and y_{hd} is its desired position. Also weight of leg torque $\tau_2 \sim \tau_4$ is tuned by setting $k_{h1} \sim k_{h3}$ of $\boldsymbol{K}_h$ presented as Eq. (28).

$$\boldsymbol{\tau} = \boldsymbol{K}_h \boldsymbol{J}_h^T \boldsymbol{f}_h \quad (\text{If} \quad q_3 \ge 1.0[rad]) \tag{26}$$

$$\boldsymbol{f}_h^T = [0,\, k_{ph}\,(y_{hd} - y_h)\,,\, f_{hz}] \tag{27}$$

$$\boldsymbol{K}_h = diag[k_{h1}, k_{h2}, k_{h3}, 1, \cdots, 1] \tag{28}$$

$$\tau_i = k_{dh}(0 - \dot{q}_i) \quad (\text{If} \quad q_3 < 1.0[rad]) \tag{29}$$

When knee joint angle drops to below 1.0 [rad], torques trying to still robot as Eq. (29) is given to each

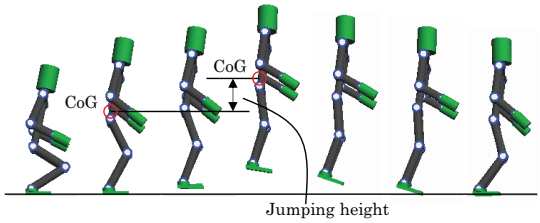

Fig. 7 Screen shot of simulation

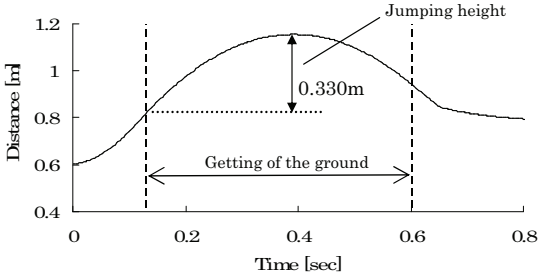

Fig. 8 Center of gravity z_g

joint and thereby robot jumps using ground reaction. k_{dh} is differential gain.

After both feet detach from the ground, PD controller presented as Eq. (30) is used for maintaining desired pose in the air. k_{pp} is proportional gain, k_{dp} is differential gain and q_{di} is desired joint angle.

$$\tau_i = k_{pp}(q_{di} - q_i) + k_{dp}(0 - \dot{q}_i) \tag{30}$$

Input torque for landing is presented as Eq. (31). $\boldsymbol{K}_{pl}$ is proportional gain, $\boldsymbol{K}_{dl}$ is differential gain and r_d is desired head position.

$$\boldsymbol{\tau} = \boldsymbol{J}_h^T(\boldsymbol{K}_{pl}(\boldsymbol{r}_d - \boldsymbol{r}) + \boldsymbol{K}_{dl}(\boldsymbol{0} - \dot{\boldsymbol{r}})) \tag{31}$$

4.2 Jumping Simulation

Each parameter is set up as follows, and jumping simulation without arms' swing was conducted.

Jumping

$k_{ph} = 20.0,\ y_{hd} = 0.5[m],\ f_{hz} = 300[N]$

$k_{h1} = k_{h2} = k_{h3} = 4.0,\ k_{dh} = 30$

In the air

$k_{pp} = 30,\ k_{dp} = 3$

$q_{di} = [q_{d2}, \cdots, q_{d8}, q_{d15}]$

$= [0.1, 0.4, -0.6, 0.6, -0.4, -0.1, 0.0, 0.0]$

Landing

$\boldsymbol{K}_{pl} = diag[0, 500, 1700],\ \boldsymbol{K}_{dl} = diag[0, 100, 500]$

$\boldsymbol{r}_d = [0.0, -0.2 + d_2, 1.9]^T$

Figure 8 shows time profile of center of gravity [CoG] excluding both arms. Here, we define jumping height in Fig. 8 as between position of CoG at the moment that both feet detach from the ground and position of CoG in the most highest position.

Next jumping simulation with arms' swinging was conducted. Arms's input torques are given as follows.

Table 1 Jumping height and time of getting off the ground

t_a [sec]	Jumping height [m]	Time of getting off [sec]
No swinging	0.330	0.132
0.00	0.375	0.141
0.02	0.347	0.138
0.04	0.320	0.135
0.06	0.313	0.135

If $t_a \le t < t_a + 0.12$

$\tau_{11,14} = 100,\ \tau_{12,15} = 60,\ \tau_{13,16} = 10$ [N · m] (32)

If $t_a + 0.12 \le t < t_a + 0.17$

$\tau_{11,14} = -150,\ \tau_{12,15} = -75,\ \tau_{13,16} = -10$ [N · m] (33)

Equation (32) represents the input torque for swinging up of arms, and Eq. (33) represents it for making arms stop at head's height. t_a is a time of starting in swinging motion. These input torques were determined through a trial-and-error processes in such a way as to make the arms' swinging motion be similar to those jumping with arms motions. The value of t_a is swept in step of 0.02 [sec] within a range from 0.00 to 0.06 [sec]. Jumping height rises as compared to without arms' swinging in $t_a = 0.00, 0.02$ [sec], but it comes down in $t_a = 0.04, 0.06$ [sec]. Also in each case with swinging arms', time of getting off the ground is later. Furthermore if time of starting in swinging motion is faster, jumping height is higher and time of getting off the ground is later.

Normal force to supporting foot and CoG are depicted in Figs. 9∼12. Both feet get off the ground from $t = 0.13$ [sec] to $t = 0.15$ [sec] and normal force becomes zero at this time. Also in landing motion, each foot bumps the ground by heel and tiptoe in that order after $t = 0.6$ [sec], and a greater impulsive force $F_{imz}/3.0 \times 10^{-3}$ arises between tiptoe and the ground. Motion energy is depicted in Figs. 13∼16. Figures 9∼16 shows that normal force and motion energy last getting off the ground rise when jumping height rises. This conclusion is considered that normal force rises and time of getting off the ground becomes late by interference of arms' swinging and thereby impulse and motion energy rises and jumping height rises.

5. CONCLUSION

We discussed arms' influence to vertical jumping motions of humanoid whose dynamics have varieties of gaits including surface-contacting and point-contacting. Simulation results indicate that normal contacting force to the ground and motion energy at the detaching moment rise and them jumping height becomes high.

Also, impulsive force in landing is smaller when time of getting off the ground is lator. It is because landing posture of the robot are influenced by arms' swinging. Thus, we think it is possible that a load of each link in landing are reduced by giving effectual input torque to each link of arms.

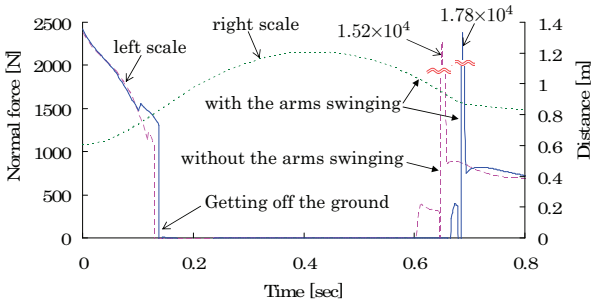

Fig. 9 Normal force and CoG z_g ($t_a = 0.00$)

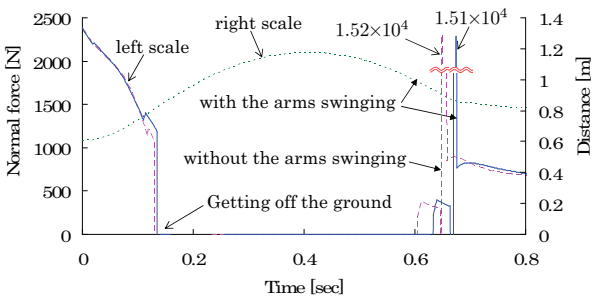

Fig. 10 Normal force and CoG z_g ($t_a = 0.02$)

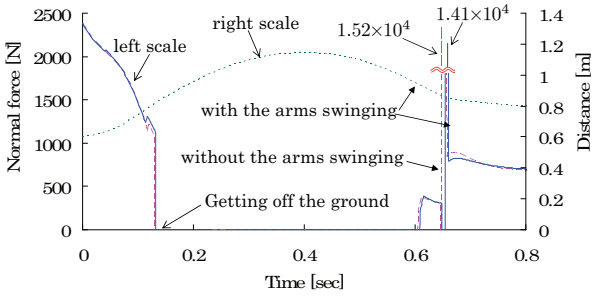

Fig. 11 Normal force and CoG z_g ($t_a = 0.04$)

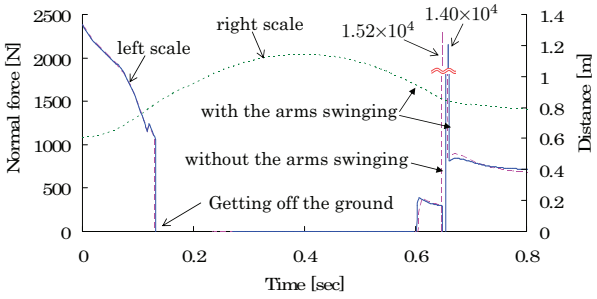

Fig. 12 Normal force and CoG z_g ($t_a = 0.06$)

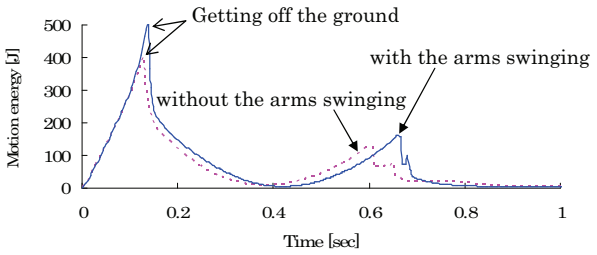

Fig. 13 Motion energy ($t_a = 0.00$)

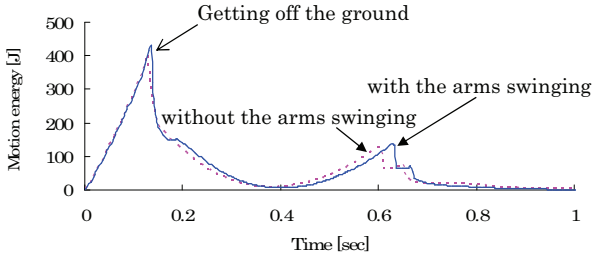

Fig. 14 Motion energy ($t_a = 0.02$)

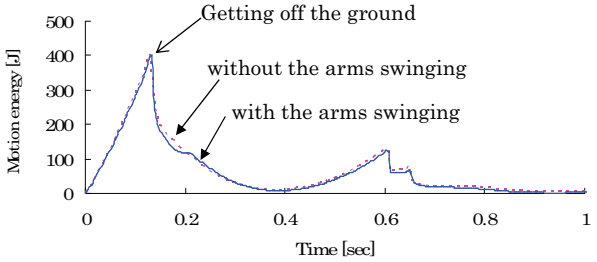

Fig. 15 Motion energy ($t_a = 0.04$)

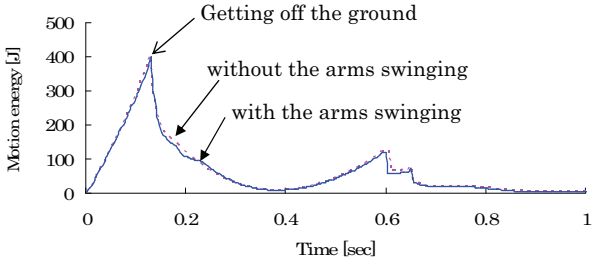

Fig. 16 Motion energy ($t_a = 0.06$)

REFERENCES

[1] Y. Huang, B. Chen, Q. Wang, K. Wei and L. Wang, "Energetic efficiency and stability of dynamic bipedal walking gaits with different step lengths," *Proc. IEEE/RSJ International Conference on Intelligent Robots and Systems*, pp.4077–4082, 2010.

[2] W. Song, M. Minami, T. Maeba. Y Zhang and A. Yanou, "Visual Lifting Stabilization of Dynamic Bipedal Walking," *Proceedings of 2011 IEEE-RAS International Conference on Humanoid Robots*, pp.345-351, 2011.

[3] J. Babic, J. Lenarcic, "Vertical Jump: Biomechanical Analysis and Simulation Study," Humanoid Robots: New Developments, pp.551–566, 2007.

[4] T. Spagele, A. Kistner, A. Gollhofer, "Modelling, simulation and optimisation of a human vertical jump," Journal of Biomechanics 32, pp.521–530, 1999.

[5] T. Wu, T. Yeh and B. Hsu, "Trajectory Planning of a One-Legged Robot Performing Stable Hop," *Proc. IEEE/RSJ International Conference on Intelligent Robots and Systems*, pp.4922–4927, 2010.

[6] Y. Fujimoto and A. Kawamura, "Three Dimensional Digital Simulation and Autonomous Walking Control for Eight-Axis Biped Robot," *Proc. IEEE International Conference on Robotics and Automation*, pp.2877–2884, 1995.

[7] J.Y.S. Luh, M.W. Walker and R.P.C. Paul, "On-Line Computational Scheme for Mechanical Manipulators," *ASME J. of DSME*, Vol.102, No.2, pp.69–76, 1980.